Brain, Behavior, and Immunity 49 (2015) 311–321

Contents lists available at ScienceDirect

Brain, Behavior, and Immunity

journal homepage: www.elsevier.com/locate/ybrbi

Presenilin-1 familial Alzheimer's disease mutation alters hippocampal neurogenesis and memory function in CCL2 null mice

Tomomi Kiyota *, Christine M. Morrison, Guihua Tu, Bhagyalaxmi Dyavarshetty, Robert A. Weir, Gang Zhang, Huangui Xiong, Howard E. Gendelman

Center for Neurodegenerative Disorders, Departments of Pharmacology and Experimental Neuroscience, University of Nebraska Medical Center, Omaha, NE 68198, USA

ARTICLE INFO

Article history:
Received 6 March 2015
Received in revised form 7 June 2015
Accepted 18 June 2015
Available online 22 June 2015

Keywords:
Hippocampus
Neurogliogenesis
Chemokine
Morris water maze
Long-term potentiation

ABSTRACT

Aberrations in hippocampal neurogenesis are associated with learning and memory, synaptic plasticity and neurodegeneration in Alzheimer's disease (AD). However, the linkage between them, β-amyloidosis and neuroinflammation is not well understood. To this end, we generated a mouse overexpressing familial AD (FAD) mutant human presenilin-1 (PS1) crossed with a knockout (KO) of the CC-chemokine ligand 2 (CCL2) gene. The PS1/CCL2KO mice developed robust age-dependent deficits in hippocampal neurogenesis associated with impairments in learning and memory, synaptic plasticity and long-term potentiation. Neurogliogenesis gene profiling supported β-amyloid independent pathways for FAD-associated deficits in hippocampal neurogenesis. We conclude that these PS1/CCL2KO mice are suitable for studies linking host genetics, immunity and hippocampal function.

1. Introduction

The *APP*, *PSEN1* and *PSEN2* genes are linked to early-onset familial Alzheimer's disease (FAD) (McKhann et al., 2011). Although numerous autosomal gene mutations have been identified, *PSEN1* is the most common (see the AD&FTD Mutation Database, http://www.molgen.ua.ac.be/admutations). Most of *PSEN1* mutations are missense. FAD mutations affect aggregation-prone forms of amyloid-β peptide (Aβ). These serve to accelerate senile plaque formation (De Strooper et al., 2012). Presenilin 1 and 2 (referred to as PS1 and PS2) are a catalytic subunit of γ-secretase complex, an aspartyl protease that cleaves type-I transmembrane proteins including amyloid-β precursor protein (APP), Notch receptors and ligands, ErbB4 and others (Koo and Kopan, 2004). Autolysosomal proteolysis processes amyloidgenic APP, and PS1 FAD mutations disrupt autolysosomal function, leading to increased Aβ production and memory loss (Lee et al., 2010; Nixon, 2013).

γ-Secretase plays a pivotal role in cell fate during embryonic and adult neurogenesis. PS1 contributes to neurogliogenesis as a component of the γ-secretase complex and is ubiquitously expressed in the brain (Ables et al., 2011; Yoon and Gaiano, 2005). Interestingly, mouse models of FAD-linked PS1 mutations affect neurogenesis by altering cell proliferation and survival (Choi et al., 2008; Veeraraghavalu and Sisodia, 2013; Zhang et al., 2007). However, how neurogenesis is affected remains undefined.

The CC-chemokine ligand 2 (CCL2), also known as monocyte chemotactic protein-1, is a β-chemokine responsible for recruitment of myeloid-lineage (monocyte-macrophages and microglia) during infectious and inflammatory diseases (Shi and Pamer, 2011). In AD, CCL2 levels are elevated in plasma, cerebrospinal fluid and the brain (Ishizuka et al., 1997; Sun et al., 2003). While Aβ stimulates microglia and astrocytes leading to CCL2 production (El Khoury et al., 2003), deficiencies of CCL2 and its ligand binding receptor, CCR2, underlie disease onset and tempo (El Khoury et al., 2007; Kiyota et al., 2013; Naert and Rivest, 2011). Such findings strongly support a role for chemokine signaling in AD pathogenesis. Indeed, CCL2 deficiency accelerates impairments in hippocampal neurogenesis, learning and memory in AD mice overexpressing human APP and PS1 with FAD mutations (Kiyota et al., 2013).

We now posit that combinations of CCL2 deficiency and PS1 FAD mutations provide synergistic effects on brain function relevant to neurogenesis-associated repair and regenerative processes. Mice overexpressing human PS1 M146L mutant, but not human APP FAD mutant, were used to assess the role in hippocampal neurogenesis activities, independent of Aβ production, aggregation and plaque formation. To such an end, mice overexpressing FAD-mutant PS1 with the CCL2 gene knocked-out (PS1/CCL2KO) were employed. Most notably the studies show, for the first time, age-dependent impairments in hippocampal neurogenesis,

* Corresponding author at: Department of Pharmacology and Experimental Neuroscience, University of Nebraska Medical Center, 985930 Nebraska Medical Center, Omaha, Nebraska 68198-5930, USA. Tel.: +1 402 559 8965.
E-mail address: tkiyota@unmc.edu (T. Kiyota).

http://dx.doi.org/10.1016/j.bbi.2015.06.014
0889-1591/

learning and memory functions that are linked to deficits in long-term potentiation (LTP) but independent of β-amyloidosis and neuroinflammatory responses. Considering these findings, the PS1/CCL2KO mouse can be useful in investigating FAD-associated deficits in hippocampal function.

2. Materials and methods

2.1. Transgenic mice

PS1 mice overexpressing human PS1 with FAD-linked mutation (M146L line 6.2) were provided by Dr. K. Duff through University of South Florida (Duff et al., 1996). CCL2KO mice [B6.129S4-Ccl2tm1Rol/J] were purchased from the Jackson Laboratory, Bar Harbor, ME, USA. Both mice were maintained in a B6.129 hybrid background (Kiyota et al., 2009, 2013). Male PS1 mice were crossed with female CCL2KO mice to generate PS1/CCL2$^{+/-}$, followed by back-cross with CCL2KO mice to generate PS1/CCL2KO mice. B6.129 hybrid non-Tg mice were bred in parallel as age-matched control. All animal studies adhered to the guidelines established by the Institutional Animal Care and Use Committee at University of Nebraska Medical Center.

2.2. Bromodeoxyuridine (BrdU) administration and tissue preparation

BrdU was intraperitoneally injected (50 mg/kg of body weight) twice daily every 12 h for 2.5 days to label proliferating cells (Butovsky et al., 2006). Three weeks after the first BrdU injection, mice were euthanized with isoflurane and perfused transcardially with 25 ml of ice-cold PBS. The brains were rapidly removed. The left hemisphere was immediately dissected and separated into three parts: cortex, hippocampus and remainder, and frozen on dry ice for biochemical testing. The right hemisphere was immersed in freshly depolymerized 4% paraformaldehyde for 48 h at 4 °C, and protected by successive 48-h immersions in 30% sucrose in 1× PBS. The fixed, cryopreserved brains were sectioned coronally using a Cryostat (30 μm, Leica, Bannockburn, IL, USA) with serial sections collected and stored at −80 °C for immunohistochemical tests.

2.3. Neural progenitor cell (NPC) cultivation

NPCs were prepared using NeuroCult Proliferation Kit (StemCell Technologies, Vancouver, BC, Canada) according to a manufacture's instruction. In brief, mouse cortices were dissected at embryonic day 14 and meninges were removed in ice-cold PBS with 2% glucose. The cortices were mechanically dissociated, filtered with a 40 μm-cell strainer and cultured as neurospheres for 3–5 days in NeuroCult Proliferation media with supplement and epidermal growth factor (20 ng/ml) (StemCell Technologies, Vancouver, BC, Canada). The neurospheres were collected and dissociated to single cells using NeuroCult Chemical Dissociation Kit (StemCell Technologies, Vancouver, BC, Canada). The cells were seeded into poly-D-lysine (100 μg/ml)/laminin (15 μg/ml) (Sigma–Aldrich, St. Louis, MO)-coated 96-well tissue culture plates at a density of 50,000 cells/well.

2.4. BrdU incorporation assay

NPCs were plated in poly-D-lysine/laminin-coated black/clear bottom 96-well microplates at a density of 50,000 cells/well, and cultured in NeuroCult Proliferation media containing BrdU (10 μM). After incubation for days as indicated, NPCs were fixed with freshly depolymerized 4% paraformaldehyde, incubated with 2 N HCl to denature DNA, neutralized with 0.1 M sodium borate, and subjected to a standard immunofluorescence using FITC-conjugated anti-BrdU antibody (Ab) (mouse monoclonal, 6 μg/ml, Roche Diagnostics, Indianapolis, IN, USA). Fluorescent intensities for BrdU uptake were measured by SpectraMAX M5 microplate reader (Molecular Devices, Sunnyvale, CA, USA) at excitation and emission wavelengths (Ex/Em) of 488/519 nm for Alexa Fluor®488 and 350/461 nm for DAPI.

2.5. Immunohistochemistry

Immunohistochemistry was performed as previously described (Kiyota et al., 2013, 2011) using specific Abs to identify doublecortin (Dcx, goat polyclonal, 1:500, Santa Cruz Biotechnology, Santa Cruz, CA, USA) and c-fos (rabbit polyclonal, 1:5000, Calbiochem, Gibbstown, NJ). Immunodetection was visualized using biotin-conjugated anti-goat or anti-rabbit IgG as a secondary Ab, followed by incubation with Vectastain ABC Elite kit (Vector Laboratories, Burlingame, CA, USA) and 3,3′-diaminobenzidine (DAB) substrate kit (Vector Laboratories, Burlingame, CA, USA). Images were captured using DP Controller and DP Manager with a DP71 digital camera (Olympus, Orangeburg, NY, USA) attached to a Nikon Eclipse TE300 inverted microscope (Nikon, Melville, NY, USA).

2.6. Immunofluorescence

Immunofluorescence was performed as previously described (Kiyota et al., 2013, 2011). Brain sections were co-incubated with FITC-conjugated anti-BrdU (mouse monoclonal, 6 μg/ml, Roche Diagnostics, Indianapolis, IN, USA) and biotin-conjugated anti-NeuN (mouse monoclonal, 1:500, Millipore, Billerica, MA, USA), or anti-s100β (rabbit polyclonal, 1:2000, Abcam, Cambridge, MA, USA), followed by incubation with Streptavidin-Alexa Fluor®568 (1:1000, Invitrogen, Carlsbad, CA, USA) or Alexa Fluor®568-conjugated anti-rabbit IgG (H + L, 1:1000). For calbindin, brain sections were incubated with anti-calbindin D-28k (rabbit polyclonal, 1:20,000, Swant, Bellinzona, Switzerland), followed by incubation with Alexa Fluor®568-conjugated anti-rabbit IgG (H + L) (1:1000) and mounted with Vectashield-DAPI (Vector Laboratories, Burlingame, CA, USA). Images in the dentate gyrus (DG) of the hippocampus were captured using a Nuance EX multispectral imaging system (Cambridge Research & Instruments, Woburn, MA, USA). Calbindin/DAPI images were pre-processed with standard outputs to a spectral library using Nuance software. Data were then quantified with ImageJ software (NIH, Bethesda, MD, USA) by separating color channels and converting to grayscale to obtain red (calbindin) and blue (DAPI) staining intensities in the dentate gyrus (DG) of the hippocampus. Calbindin positive areas were normalized to DAPI intensity to ensure standardization of differences amongst experimental conditions. Seven brains/mice per group were analyzed.

2.7. Stereological quantification

We defined cell bodies with DAB signals in the subgranular zone (SGZ) of the DG as Dcx$^+$ cells (Couillard-Despres et al., 2005), cells with DAB-stained nuclei in the granular cell layer (GCL) of the DG as c-fos$^+$ cells, and cells that have both FITC and Alexa Fluor®568 (NeuN or Gfap) signals in the dentate SGZ as BrdU$^+$/NeuN$^+$ or BrdU$^+$/Gfap$^+$ cells (Kiyota et al., 2011). Positive cells were counted in a blinded fashion in every 8th section through the entire anterio–posterior extent of the DG (total 12 sections per hippocampus) and estimated using stereological analysis with Stereo Investigator system with an optical fractionator module (MBF Bioscicence, Williston, VT). The system consisted of a high

sensitivity digital camera (OrcaFlash2.8, Hamamatsu C11440-10C, Hamamatsu, Japan) interfaced with a Nikon Eclipse 90i microscope (Nikon, Melville, NY, USA). Within the Stereo Investigator program, the contour of DG of each section was delineated using a tracing function. While sections showed shrinkage along the anterio–posterior axis, the extent of shrinkage between different animals was similar. The dimensions for the counting frame (450 × 450 μm) and the grid size (500 × 500 μm) were set. The *z*-plane focus was adjusted at each section for clarity, and images were automatically acquired according to each setting. Based on these parameters and marked cell counts, the Stereo Investigator program by fractionator module computed the estimated cell population. The estimated population, cell counts and the Gunderson ($m = 1$) values were recorded for each animal and compared between groups using a statistical software (Prism 4.0, Graphpad Software, San Diego, CA).

2.8. NPC immunofluorescence

Cultured NPCs were chilled on ice, fixed with freshly depolymerized 4% paraformaldehyde for 15 min at room temperature, washed with PBS three times, and subjected to a standard immunofluorescence using Abs to MAP2 (mouse monoclonal, 1:1000, Millipore, Billerica, MA, USA), GFAP (rabbit polyclonal, 1:2000, DAKO, Carpenteria, CA, USA), TuJ1 (β-Tubulin III, mouse monoclonal, 1:1000, Sigma, St. Louis, MO USA), s100β (rabbit polyclonal, 1:2000, Abcam, Cambridge, MA, USA). Alexa Fluor®488 or 568-conjugated anti-mouse or rabbit IgG (1:1000) was used as a secondary Ab, followed by 30-min counterstaining with DAPI (all from Invitrogen, Carlsbad, CA, USA).

2.9. Morris water maze task

The Morris water maze (MWM) task was run to assess spatial learning and memory performance of the mice as described with minor modifications (Arendash et al., 2006). Mice were introduced into the perimeter of a circular water-filled tank (21–22 °C) 110 cm in diameter and 91 cm in height (San Diego Instruments, San Diego, CA) with visual cues that were present on the tank walls as spatial references. The tank was divided into four equal quadrants (Q1–4) by lines drawn on the floor. A 10 cm circular plexiglass platform was submerged 1 cm deep in Q2 and as such hidden from the mice. The mice started the task from one of three quadrants excluding Q2. Four trials were performed per mouse per day for 10 days. Each trial lasted 1 min and ended when the mouse climbed onto and remained on the hidden platform for 10 seconds. The mouse was given 20 s to rest on the platform between trials. The time taken by the mouse to reach the platform was recorded as its latency. If the mouse did not reach the platform, 60 s was recorded as its latency and the mouse was gently guided to the submerged platform. The time for four trials was averaged and recorded as a result for each mouse. On day 11, the mice were subjected to a single 60-s probe trial without platform for memory retention. After each trial, mice were gently wiped using paper towels to remove aqueous droplets then put back into cages on a warming pad. The mice started the trial from Q4, the number of annulus crossings was counted, and swimming path was recorded using an overhead video camera and Ethovision tracking software (Noldus Information Technology, Leesburg, VA, USA). The percent of time spent in each quadrant was calculated using the software.

2.10. RNA extraction and transcript analyses

Total RNA was extracted from the hippocampus of each mouse using a Dounce homogenizer and the RNeasy Mini Kit (Qiagen, Valencia, CA, USA). For PCR-based transcript analysis, cDNA from non-Tg and PS1/CCL2KO mice was synthesized with 1 μg of total RNA as a template using the RT2 First Strand Kit (Qiagen, Valencia, CA, USA), and quantitative real-time RT-PCR (RT2-qPCR) was performed on a thermocycler (Mastercycler Gradient, Eppendorf Scientific Inc., Westbury, NY, USA) using Mouse Neurogenesis RT2 Profiler PCR Array (Qiagen, Valencia, CA, USA) according to the manufacturer's instruction. Gene expression was calculated and visualized as a color clustergram using RT2 Profiler PCR Array Data Analysis version 3.5 (http://pcrdataanalysis.sabiosciences.com/pcr/arrayanalysis.php?target=upload, Qiagen, Valencia, CA, USA). For conventional RT2-qPCR-based gene expression analysis, 1 μg of total RNA from the hippocampus of each mouse was reverse-transcribed using Superscript II (Invitrogen, Carlsbad, CA, USA), and RT2-qPCR was performed on the thermocycler using RT2 SYBR Green qPCR Master Mix (Qiagen, Valencia, CA, USA) and gene specific primer sets (forward and reverse) as follows; *Nog* (5′-GCCAGCACTATCTACACATCC and 5′-GCGTCTCGTTCAGATCCTTCTC), *Fgf2* (5′-GCGACCCACACGTCAAACTA and 5′-TCCCTTGATAGACACAACTCCTC), *Neurod1* (5′-ATGACCAAATCATACAGCGAGAG and 5′-TCTGCCTCGTGTTCCTCGT), and *Gapdh* (5′-AGGTCGGTGTGAACGGATTTG and 5′-TGTAGACCATGTAGTTGAGGTCA). Thermal cycler condition was as follows: 10 min at 95 °C for activation of polymerase, followed by 40 cycles of a two-step PCR (95 °C for 15 s and 60 °C for 1 min). Relative expression for target genes was determined by the ΔΔCT method, and normalized with Glyceraldehyde-3-phosphate dehydrogenase (Gapdh) gene expression as an internal control.

2.11. Hippocampal slices and electrophysiological recordings

Mouse hippocampal electrophysiology was performed as previously described (Anderson et al., 2004). Briefly, mice were anesthetized with isoflurane and decapitated at 7 months of age. The brains were quickly removed from the cranial cavity and placed into an ice-cold (4 °C) pre-oxygenated artificial cerebrospinal fluid (ACSF). Hippocampi were dissected out and transverse hippocampal slices (400 μm in thickness) were cut using a tissue chopper. Slices were kept in a humidified/oxygenated holding chamber at room temperature for at least 1 h before being transferred to a recording chamber. In the recording chamber, single hippocampal slices were submerged and continuously perfused (2.0 ml/minute) with ACSF containing (in mM): NaCl (124.0), KCl (3.0), $CaCl_2$ (2.0), $MgCl_2$ (2.0), NaH_2PO_3 (1.0), $NaHCO_3$ (26.0) and glucose (10.0), equilibrated with 95% O_2 and 5% CO_2, pH 7.35–7.45. The temperature of the perfusate was maintained at 30 ± 1 °C with an automatic temperature controller (Warner Instrument Corp., Hamden, CT). Field excitatory postsynaptic potentials (fEPSPs) were elicited by a constant current stimulation (0.05 Hz, 40–120 μA) of Schaffer collateral-commissural axons using an insulated bipolar tungsten electrode. Intensity and duration of stimulation were adjusted to generate approximately 30–40% of a maximal response. Evoked fEPSPs were recorded in the CA1 dendrite field (stratum radium) with borosilicated glass microelectrodes, which had a tip diameter of 2.5–5.0 μ and a resistance of 1–5 MΩ when filled with ACSF and amplified with an Axopatch-1D amplifier and a Dagan EX4-400 amplifier. Each recording trial was an average of 3 consecutive sweeps. High frequency stimulation (HFS, 100 Hz, 500 ms) was delivered twice in 20-s intervals at the same intensity as that employed in test pulses (low frequency). Electrical signals were filtered at 1 kHz and digitized at a frequency of 5 kHz using a Digidata 1320 interface (Axon Instruments, Inc.). Data were stored on a desktop PC and analyzed off-line using pCLAMP 10 software (Axon Instruments, Inc.). The initial slope of the fEPSPs was analyzed and expressed in percentage of basal level. In bar graphs, the magnitudes of LTP were quantified from 50 to 60 min after HFS.

2.12. Statistics

All data were normally distributed and presented as mean values ± standard errors of the mean (SEM). In case of multiple mean comparisons, the data were analyzed by one-way ANOVA and Newman–Keuls post hoc or two-way repeated measures ANOVA, followed by Bonferroni multiple comparison tests using statistics software (Prism 4.0, Graphpad Software, San Diego, CA). For LTP, data were analyzed by two-tailed *t*-test. A value of $P < 0.05$ was regarded as a significant difference.

3. Results

3.1. PS1/CCL2KO mice show impaired adult hippocampal neurogenesis

Impairment in hippocampal neurogenesis is associated with the CCL2KO APP/PS1 mouse phenotype. However, the CCL2KO phenotype alone is not associated with changes in numbers of proliferating cells or neuronal survival (Kiyota et al., 2013). Whether FAD mutations, which affect learning and memory, are linked to deficits in hippocampal neurogenesis is incompletely understood. However, the nature of such associations is certainly critical for understanding AD pathobiology. Such information could provide insights into disease processes independent of Aβ formation. To this end, we bred human PS1 M146L mutant-overexpressing (PS1 mice), CCL2KO mice and PS1/CCL 2KO mice while non-transgenic (Tg) mice were propagated as controls. The PS1/CCL2KO mice did not show any growth abnormalities or alterations in body or brain weight and sex ratio at delivery (Supplementary Table 1).

To decipher the links between specific genetic mutations and disease, we examined doublecortin (Dcx) expression within the hippocampus. Dcx is a marker for newly generated premature neurons in the SGZ of the DG serving as a reliable screen for neurogenesis. Notably, the numbers of Dcx^+ cells in PS1/CCL2KO mice were minimally decreased with no significant changes at 4 months of age (Fig. 1A and C). However, Dcx^+ cell numbers were significantly reduced at 7 months of age (Fig. 1B and D). To substantiate these results, cell proliferative and differentiating responses in the SGZ were examined following intraperitoneal injections of BrdU 3 weeks prior to study end. This enabled tracking of neural differentiation ($NeuN^+/BrdU^+$ cells). Total $BrdU^+/NeuN^+$ cells in the SGZ were decreased in PS1/CCL2KO mice (Fig. 2A and B). To examine if genetic modification affected cell proliferation, neural progenitor cells (NPCs) were isolated from all animal groups and cultured with BrdU, followed by a BrdU incorporation assay. No difference in BrdU incorporation was observed between transgenic mouse lines (Fig. 2C). However, NPCs cultivation showed that numbers of $MAP2^+$ and $TuJ1^+$ cells were significantly decreased in *in vitro* differentiated NPCs from PS1/CCL2KO mice (Fig. 2D–F, H). In contrast, numbers of glial fibrillary acidic protein $(GFAP)^+$ cells were increased (Fig. 2D and G). Since GFAP is expressed both in astrocytes and neural stem cells (Kempermann et al., 2004), s100β was used as a secondary glial cell marker (Choi et al., 2008). $s100\beta^+$ cells were

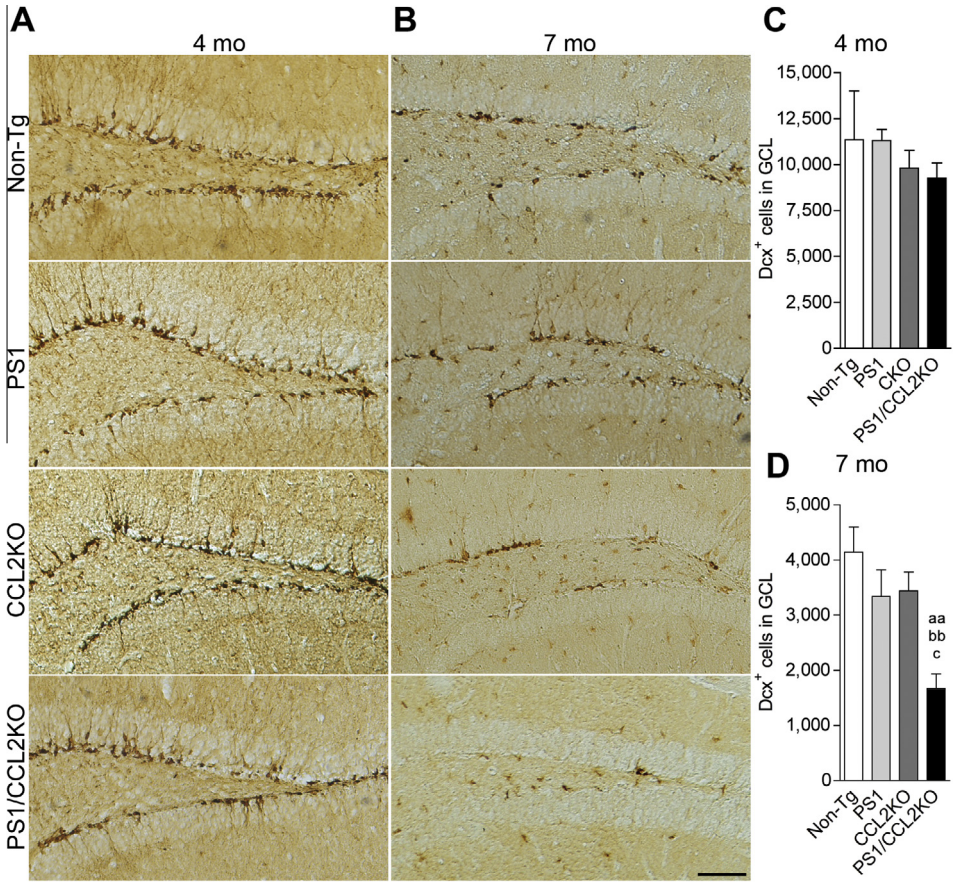

Fig. 1. Overexpression of a PS1 FAD mutant in CCL2-null mice results in fewer newborn neurons in the DG of the hippocampus. (A and B) Immunohistochemical detection of Dcx-labeled cells in the DG from 4-month-old (A) and 7-month-old (B) mice. Scale bar, 100 μm. (C and D) Quantification of the number of Dcx-labeled cells in the DG from 4-month-old (C) and 7-month-old (D) mice ($n = 7$ mice per group, 12 sections per mouse, $P = 0.6728$ (C) and 0.0016 (D)). Data are presented as mean ± SEM $^{aa,bb}P < 0.01$ vs non-Tg or PS1, $^{c}P < 0.05$ vs CCL2KO, one-way ANOVA, Newman–Keuls post hoc test.

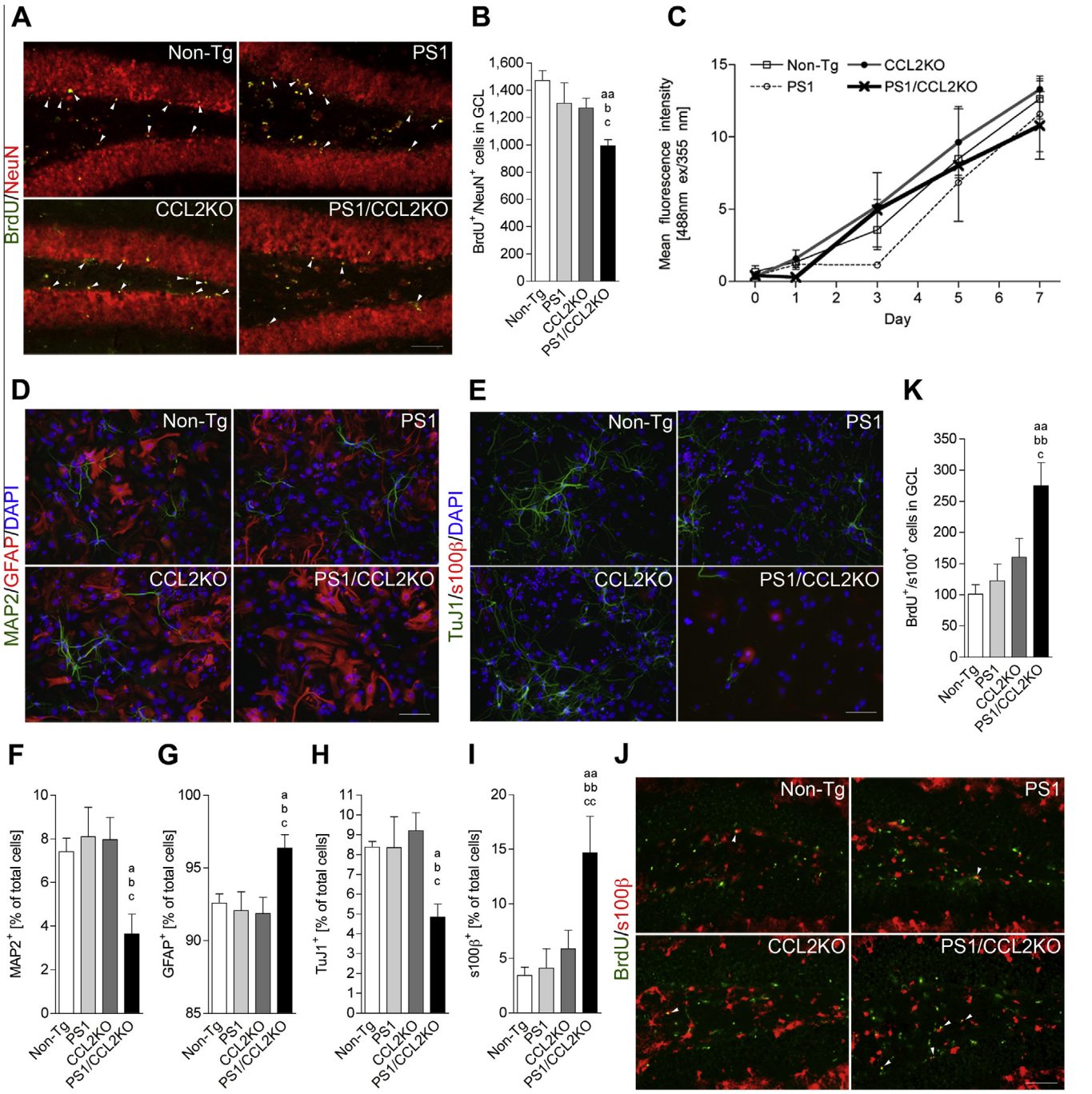

Fig. 2. Overexpression of a PS1 FAD mutant in CCL2-null mice results in reduced adult neurogenesis in the dentate SGZ. (A) Immunofluorescent detection of BrdU and NeuN double-labeled cells in the SGL from 7-month-old mice. Scale bar, 50 μm. (B) Quantification of the number of BrdU and NeuN double-labeled cells in the SGL from 7-month-old mice after 3-weeks BrdU labeling ($n = 7$ mice per group, 12 sections per mouse, $P = 0.0051$). (C) No difference in BrdU incorporation between the transgenic lines. NPCs were isolated from all animal groups and cultured with BrdU. Immunofluorescence using FITC-conjugated anti-BrdU antibody was performed. Quantification of BrdU fluorescent density shows consistent proliferation rate between all lines ($n = 3$ cultures per each group, $P = 0.7462$ as determined by two-way ANOVA, Bonferroni post hoc test). (D and E) Immunofluorescence of MAP2/GFAP (D) or TuJ1/s100β (E)-positive cells differentiated from NPCs. Scale bars, 100 μm. (F–I) Quantification of MAP2 (F), GFAP (G), TuJ1 (H) or s100β (I)-positive cells. Data are presented as the percentage of total cells in *in vitro* cultivation ($n = 3$ cultures per each group from 3 independent experiments, $P = 0.0138$ (F), 0.0137 (G), 0.0386 (H) or 0.0056 (I)). (J) Immunofluorescent detection of BrdU and s100β double-labeled cells in the SGL from 7-month-old mice. Scale bar, 50 μm. (K) Quantification of the number of BrdU and s100β double-labeled cells in the DG from 7-month-old mice after 3-weeks BrdU labeling ($n = 7$ mice per group, 12 sections per mouse, $P = 0.0015$). Data are presented as mean ± SEM $^{a,b,c}P < 0.05$ vs non-Tg, PS1 or CCL2KO, $^{aa,bb,cc}P < 0.01$ vs non-Tg, PS1 or CCL2KO, one-way ANOVA, Newman–Keuls post hoc test.

increased in PS1/CCL2KO mice (Fig. 2E and I), suggesting that NPCs from PS1/CCL2KO mice shift to a glial fate. To provide cross validation for these results, hippocampal sections were double-stained for BrdU and s100β. BrdU$^+$/s100β$^+$ double positive cells were increased in PS1/CCL2KO mice (Fig. 2J and K). Taken together, these results support the idea that these genetic modifications directly affect cell fates of newly generated neural cells.

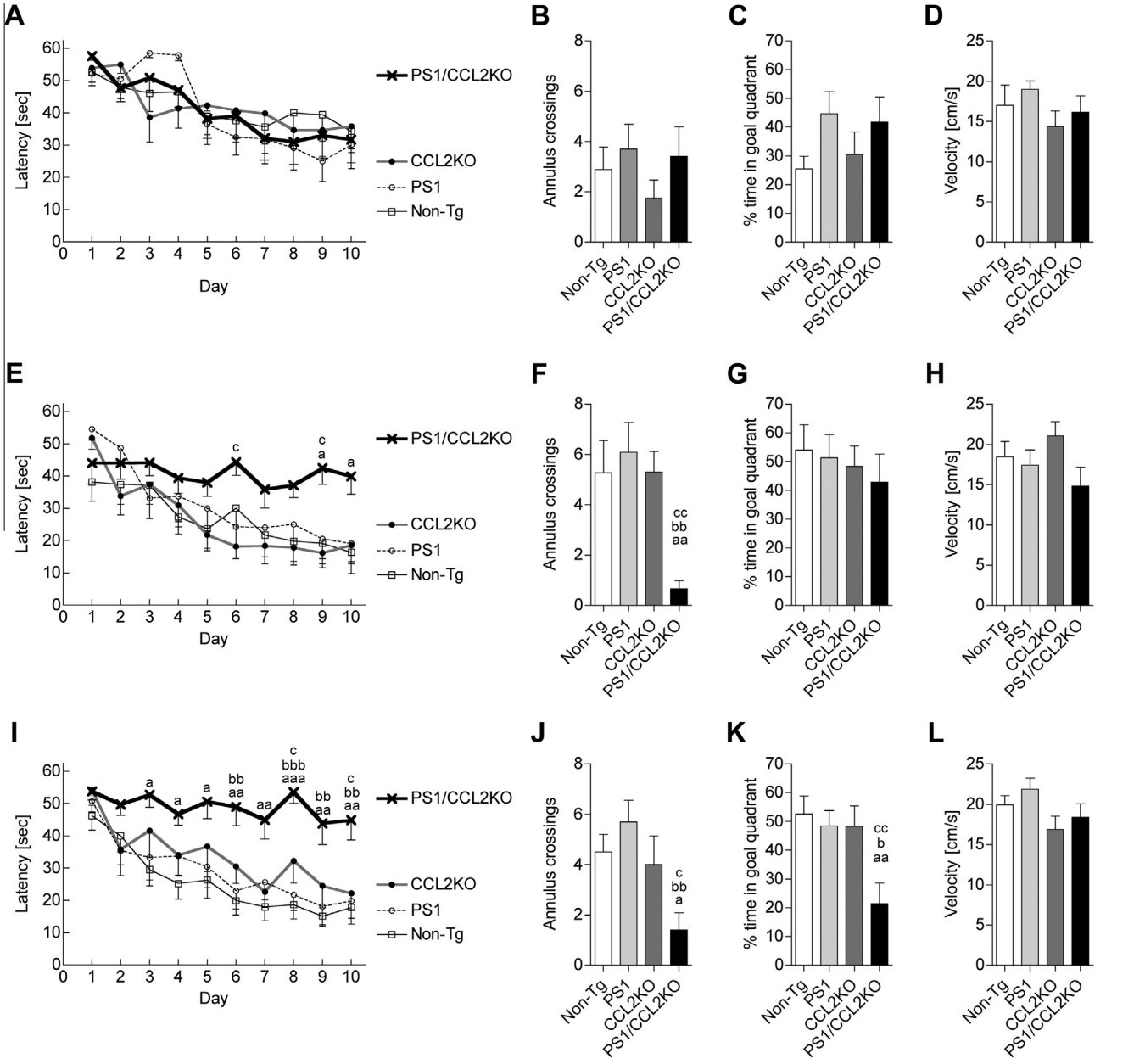

Fig. 3. Morris water maze (MWM) tasks reveal impairments in memory acquisition and retention in PS1/CCL2KO mice. (A–D) MWM task at 2 months of age shows no difference in learning and memory between the transgenic lines at both MWM acquisition phase (A) where escape latency during a 1-min trial was measured, and MWM retention phase (B and C). During a one-time probe trial after memory acquisition, number of annulus crossings (B) and duration spent in the goal quadrant between groups (C) were analyzed. (D) Measurement of average swimming speed of animals. Average swimming speeds are unchanged between groups. (E) MWM acquisition phase at 4 months of age (n = 11 (non-Tg), 10 (CCL2KO), 12 (PS1, PS1/CCL2KO)). PS1/CCL2KO mice show an initial trend to increase escape latencies as compared to other groups after day 6. (F and G) MWM retention phase. Number of annulus crossings is fewer in PS1/CCL2KO mice as compared to other groups (F), but no significant difference in duration spent in the goal quadrant between groups (G). (H) Measurement of average swimming speed of animals at 4 months of age. (I) MWM acquisition phase at 7 months of age (n = 10 (non-Tg, PS1, PS1/CCL2KO), 8 (CCL2KO)). PS1/CCL2KO mice show statistically higher escape latencies as compared to other groups. (J and K) MWM retention phase at 7 months of age. Both number of annulus crossings (J) and percent search time (K) are statistically fewer as compared to other groups. (L) Measurement of average swimming speed of animals at 7 months of age. Data are presented as mean ± SEM $^{a,b,c}P < 0.05$, $^{aa,bb,cc}P < 0.01$, $^{aaa,bbb}P < 0.001$, ^{a,aa,aaa} vs non-Tg, ^{b,bb,bbb} vs PS1, ^{c,cc} vs CCL2KO, two-way ANOVA, Bonferroni post hoc (A, E and I) or one-way ANOVA, Newman–Keuls post hoc (F, J and K) test.

3.2. PS1/CCL2KO mice demonstrate memory and learning impairments

Correlations between memory, learning and adult neurogenesis were previously investigated (Aimone et al., 2006) including within the DG of the hippocampus (Deng et al., 2010; Kiyota et al., 2011; Lledo et al., 2006). As significant changes in hippocampal neurogenesis were observed in PS1/CCL2KO mice, we investigated if such changes are linked to impairments in learning and memory. To this end, we employed a 10-day Morris water maze (MWM) task to assess learning and memory acquisition, and a 1-day probe test for memory retention. We observed no difference in memory acquisition and retention between all groups at 2 months of age (Fig. 3A–C). At 4 months of age, PS1/CCL2KO mice group showed impaired memory acquisition (Fig. 3E). This included annulus crossing in the target quadrant that contained a submerged platform observed during the memory acquisition phase (Fig. 3F). However, PS1/CCL2KO mice showed similar spatial preference amongst each of the animal groups for the target

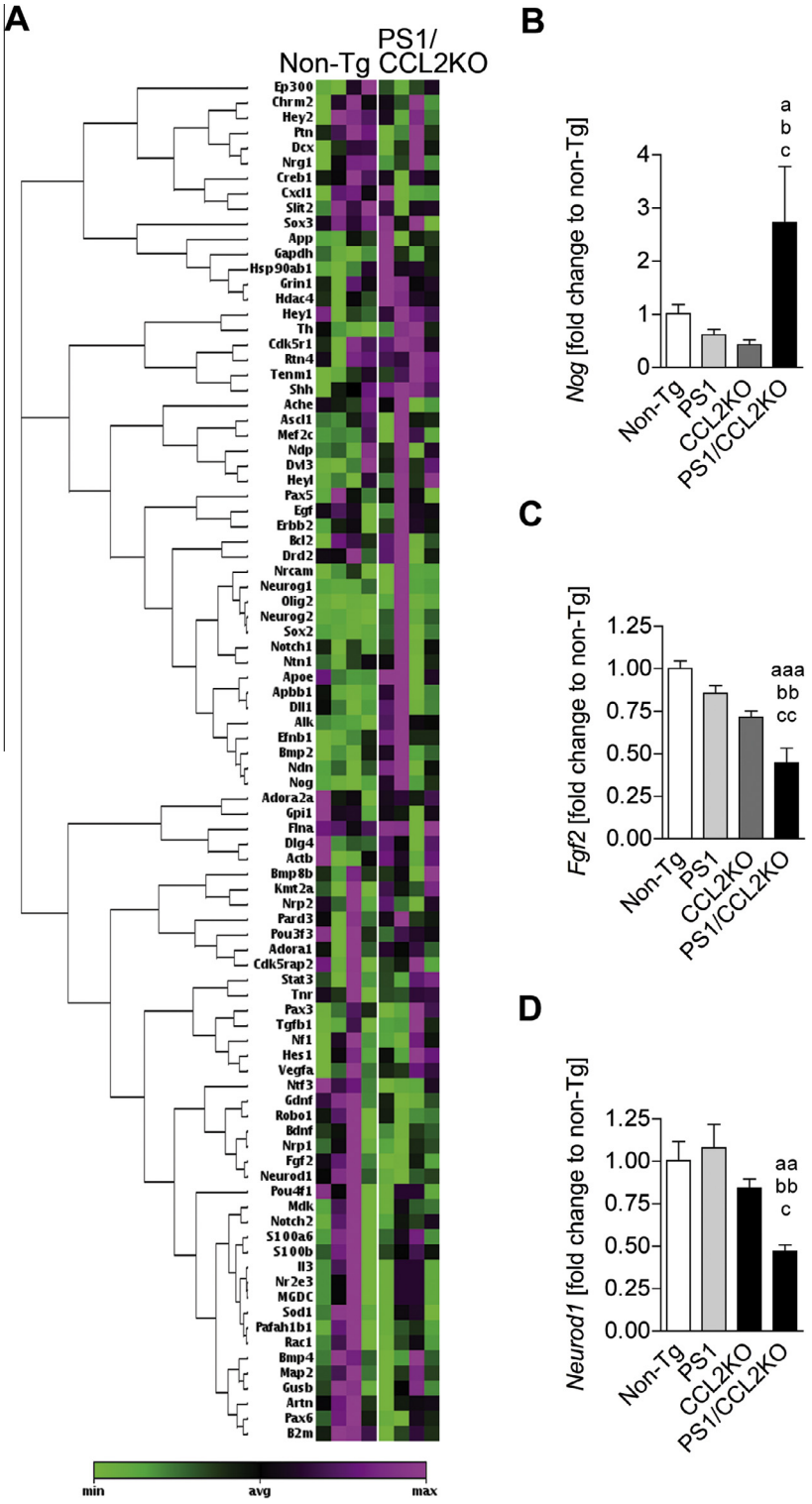

Fig. 4. Overexpression of a PS1 FAD mutant in CCL2-null mice leads to changes in hippocampal gene expression related to neurogenesis and synaptic function. (A) Heat map depicting fold changes in neurogenesis-related genes in the hippocampus between non-Tg and PS1/CCL2KO mice ($n = 4$ mice per group). Shades of green and magenta show down-regulated and up-regulated genes, respectively. (B–D) A conventional RT2-qPCR was performed to measure *Nog* (B), *Fgf2* (C) and *Neurod1* (D) expression using primer sets and synthesized cDNA with total RNA isolated from the hippocampus of each mouse ($n = 4$ mice per group, $P = 0.0392$ (B), 0.0007 (C) and 0.0029 (D)). Data are presented as mean ± SEM $^{a,b,c}P < 0.05$, $^{aa,bb,cc}P < 0.01$, $^{aaa}P < 0.001$, ^{a,aa,aaa} vs non-Tg, ^{b,bb} vs PS1, ^{c,cc} vs CCL2KO, one-way ANOVA, Newman–Keuls post hoc test. (For interpretation of the references to color in this figure legend, the reader is referred to the web version of this article.)

quadrant (Fig. 3G). At 7 month of age, PS1/CCL2KO mice group showed longer latency during a 10 day observation period (Fig. 3I), lower number of annulus crossings (Fig. 3J) and no quadrant preference (Fig. 3K), suggesting significant impairments in learning and memory. Average swimming speeds were unchanged between groups at all time points, ruling out the possibility of differences in their swimming abilities distorting the data (Fig. 3D, H and L). The data support the notion that learning and memory performance in PS1/CCL2KO mice worsen in an age-dependent manner.

3.3. Neurogenesis-related neuronal gene profiling

As deficits in learning, memory and hippocampal neurogenesis in PS1/CCL2KO mice were observed, we next investigated the molecular mechanisms underlying these observations. To this end, gene expression in the hippocampus of PS1/CCL2KO mouse group were profiled and compared to non-Tg mouse groups using a neurogenesis-linked PCR array (Fig. 4A and Supplementary data 1). Downstream genes of Notch signaling were deregulated (increase in *Hes1, Hey1*, decrease in *Ascl1*) but not to the point of statistical significance. Although neurotrophic factors (*Bdnf*, *Nt3*) that are associated with synaptic function and memory (Gao et al., 2010; Shimazu et al., 2006) were reduced, significant differences were found in decreased *Fgf2* and increased *Nog* expression in the PS1/CCL2KO mice. While most of neurogenic genes showed no change in gene expression, *Neurod1* was reduced with a significant difference in the PS1/CCL2KO mice. The genes were validated using a conventional RT-qPCR (Fig. 4B–D). Importantly, the data set supported changes in synaptic function-related genes linked to memory formation.

The proto-oncogene *c-fos* is one of the immediate-early genes that are induced by neural activity and behavior, and classically known to play a role in the neuroplastic mechanisms required for memory consolidation (Kiyota et al., 2011; Palop et al., 2003). To address if memory impairment in PS1/CCL2KO mice associated with c-fos expression, c-fos-immunoreactive (c-fos$^+$) neurons were evaluated in the dentate GCL (Fig. 5A). Importantly, the number of c-fos$^+$ neurons in PS1/CCL2KO mice was significantly reduced compared to other mice (Fig. 5C).

The calcium-binding protein calbindin-D28 k can regulate intracellular calcium levels essential for hippocampal learning and memory (Molinari et al., 1996). Therefore, we measured calbindin in the DG (Fig. 5B). The expression level of calbindin in PS1/CCL2KO mice was reduced (Fig. 5D). These data support learning and memory and synaptic gene deficits for PS1/CCL2KO mice.

3.4. LTP Impairments in PS1/CCL2KO mice

Synaptic plasticity and LTP underlie learning and memory-dependent behavior (Malenka and Bear, 2004). To assess whether PS1/CCL2KO impairs synaptic transmission we studied mouse LTP in Schaffer-collateral CA1 synaptic pathways from hippocampal brain slices (Fig. 6A). High frequency stimulation of this pathway produced robust LTP as recorded in the CA1 hippocampal region from non-Tg mice. An average magnitude of 194.8 ± 11.5% (Fig. 6B, $n = 6$, mean ± SEM) of baseline when measured from 50

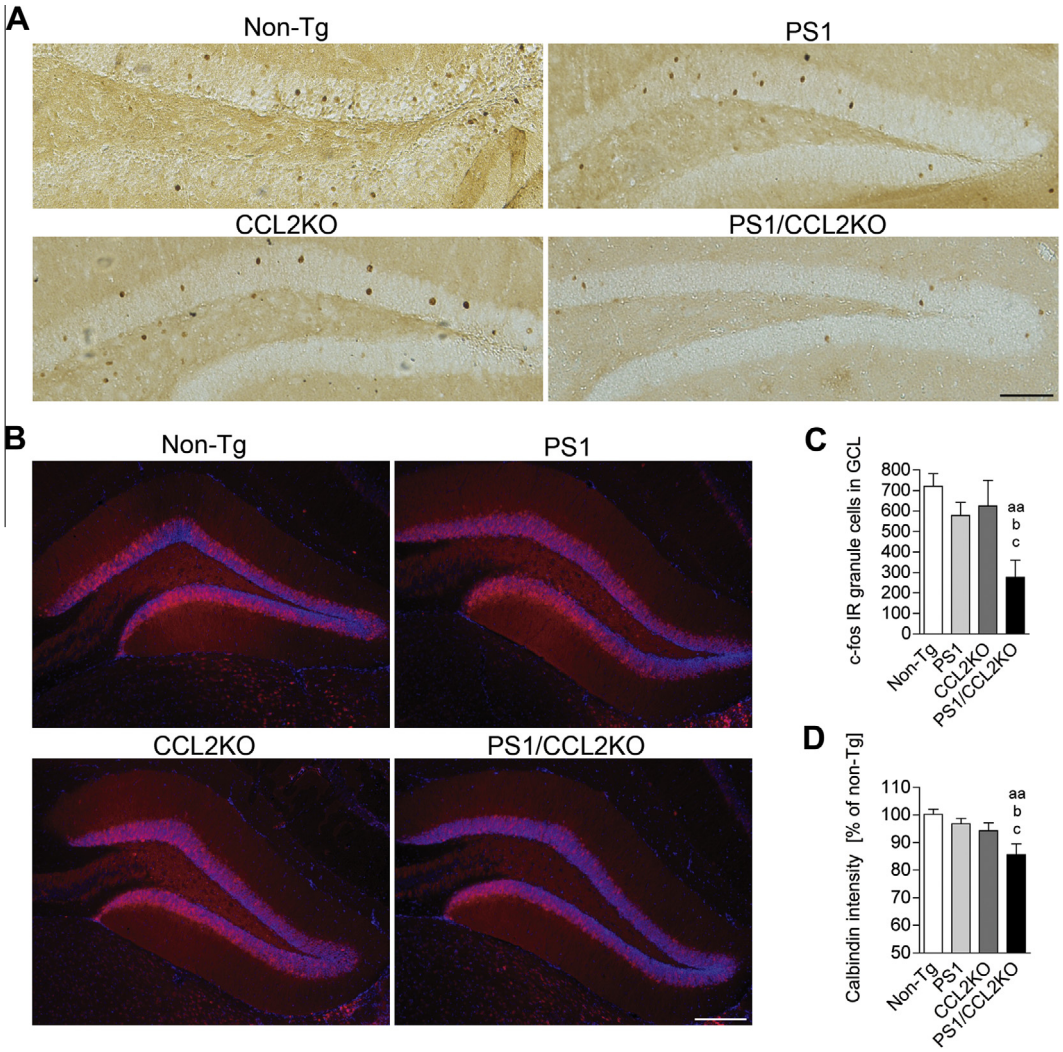

Fig. 5. Overexpression of a PS1 FAD mutant in CCL2-null mice affects expression of learning and memory-related molecules. (A) Immunohistochemical detection of c-fos-labeled cells in the dentate GCL at 7 months of age. Scale bar, 100 μm. (B) Calbindin expression in the DG of the hippocampus at 7 months of age. Scale bar, 200 μm. (C and D) Quantification of the number of c-fos-labeled cells (C, $n = 7$ mice per group, 12 sections per mouse, $P = 0.0092$) and calbindin expression levels (D, $n = 7$ mice per group, 10 sections per mouse, $P = 0.0046$). Data are presented as mean ± SEM $^{a,b,c}P < 0.05$, $^{aa}P < 0.01$, ^{a,aa} vs non-Tg, ^{b} vs PS1, ^{c} vs CCL2KO, one-way ANOVA, Newman–Keuls post hoc test.

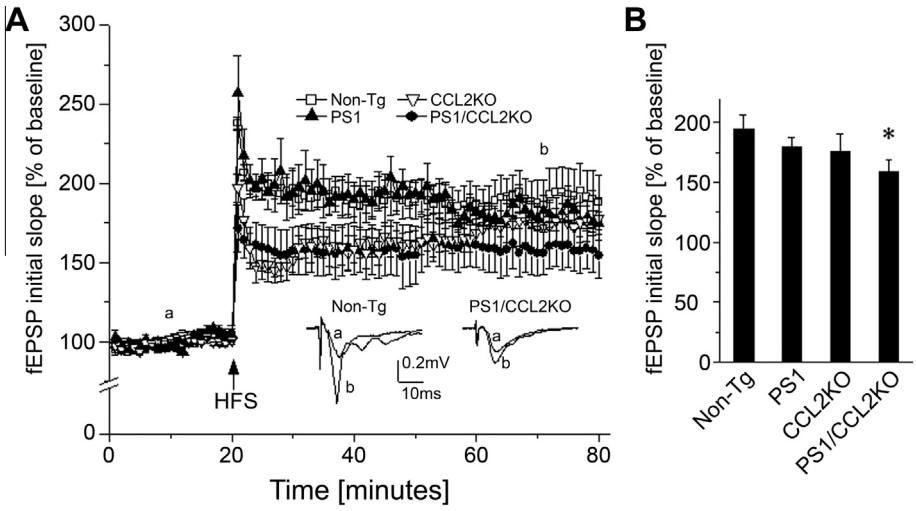

Fig. 6. LTP measures in PS1/CCL2KO mice. (A) Time courses and average magnitudes of LTP recorded in the CA1 region of hippocampal slices prepared from non-Tg (□), PS1 (▲), CCL2KO (▽) and PS1/CCL2KO (●) animals. The graph plots the initial slope of the evoked fEPSPs in response to constant current stimuli. HFS (100 Hz, 500 ms × 2) was delivered at the time indicated by an arrow. Each point in this graph represents an average of 6 slices. The representative fEPSPs taken at 10 min before and at 50 min after HFS (as indicated by letters a and b) in one of the non-Tg (left) and one of the PS1/CCL2KO (right) slices are shown below the LTP time course. Note that HFS produced a significant increase of fEPSP in non-Tg slice, but not in PS1/CCL2KO slice. (B) A bar graph showing the average LTP magnitudes measured from 50 to 60 min after HFS. Note a significant reduction of LTP magnitude in the hippocampal slices prepared from PS1/CCL2KO animals. Data are presented as mean ± SEM $^{*}P < 0.05$ vs non-Tg, two-tailed *t*-test.

to 60 min after HFS was elicited. In contrast, the average magnitude of LTP recorded in PS1/CCL2KO animals was 158.5 ± 10.3% ($n = 6$) of baseline. The difference was statistically significant ($P < 0.05$), supporting the fact that PS1/CCL2KO impairs LTP. In contrast, the average LTP magnitudes recorded in PS1 and CCL2KO animals were 179.7 ± 8.2% and 175.9 ± 14.2% of baseline, respectively. The differences were not statistically significant when compared to the average magnitude recorded in non-Tg animals.

4. Discussion

Genetically modified mice overexpressing a PS1 FAD mutant on a CCL2 null background significantly decreased hippocampal neurogenesis and affected age-dependent learning and memory. Synergy between PS1 mutation and the CCL2KO was shown. Indeed, no change in either neurogenesis or deficits in learning and memory was observed in Tg mice with single gene modifications (PS1 and CCL2KO mice). Although most Tg mice with human APP FAD mutations show impaired neurogenesis, this is explained largely by a presence of β-amyloidosis. Interestingly, divergent reports have emerged in regards to the role played by PS1 FAD mutants in NPC proliferation and survival, notably in the SGZ of the DG (Elder et al., 2010; Winner et al., 2011). PS1 P117L mutation does not affect NPC proliferation but impairs $BrdU^+$ $\beta III\text{-tubulin}^+$ neuronal survival (Wen et al., 2004). PS1 A246E mutation increases NPC proliferation but does not affect $BrdU^+/NeuN^+$ neuronal numbers (Chevallier et al., 2005). In PS1 M146L mice, no change in NPC proliferation and survival was observed (Choi et al., 2008) supporting the current study findings. However, PS1 M146L mice with CCL2 deficiency led to decreased Dcx^+ and $BrdU^+/NeuN^+$ neuronal numbers at 7 months of age. This suggests a potential synergistic effect between the PS1 mutation and the CCL2KO for hippocampal neurogenesis.

Recent studies have correlated memory function to adult neurogenesis in the DG of the hippocampus (Lee et al., 2012). Although it is still unclear if neurogenesis impairments contribute to disease progression, hippocampus-linked deficits in learning and memory formation are linked to the pathobiology of neurodegenerative disorders. Notably, AD mouse models with β-amyloidosis in the brain show memory impairment associated with impaired hippocampal neurogenesis (Zhao et al., 2008). In this study, PS1/CCL2KO mice showed impairments in learning, memory and neurogenesis despite absence of Aβ deposits and endogenous Aβ42 level that is the same as in PS1 mice, suggesting that those deficits are not due to β-amyloidosis, including Aβ toxicity, altered Aβ42/40 ratio and tau phosphorylation (Supplementary Fig. 1). In addition, we did not observe any neuroinflammatory responses that included changes in interleukin (IL)-1β, IL-6; Supplementary Figs. 2 and 3) or IL-4-mediated microglial activation (Choi et al., 2008) (data not shown), suggesting that the deficits are not due to neuroinflammation. Surprisingly we observed memory loss starting as early as 4 months of age, but only a slight decrease in the number of Dcx^+ cells in the SGZ of the DG. These data suggest that impaired learning and memory performance precedes reduced neurogenesis.

Notch signaling is a well-known conserved pathway affecting neural stem cell development (Louvi and Artavanis-Tsakonas, 2006). In the study, GFAP and $s100\beta^+$ cells rather than $NeuN^+$ and $MAP2^+$ cells were increased in the SGZ and NPCs of PS1/CCL2KO group, but the proliferation rate did not change. Thus, consideration of the signaling pathway how the NPCs are regulated is essential. Gene profiling in the hippocampus demonstrated that Notch signaling components were positively regulated, and *Neurod1* was decreased, suggesting that NPCs shift to a glial fate (astrocytes). However, we did not observe any strong distinction for those genes. The lack of the distinction might be due to a chronic but not acute response of the pathway, and indicate involvement of other regulatory systems.

Interestingly, the profiling revealed significantly increased *Nog* expression in PS1/CCL2KO mice over non-Tg control. Notably, noggin is a secreted extracellular antagonist like others, chordin and follistatin, for bone morphogenetic protein (BMP) signaling. It binds to BMP ligands to block interaction with BMP receptors, to promote neurogenesis (Gaulden and Reiter, 2008). However, our data showed decreased rather than promoted neurogenesis in PS1/CCL2KO mice as compared to other groups, suggesting that the up-regulation of noggin does not serve to inhibit BMP signaling but rather to participate in another task: the regulation of synaptic plasticity (Sun et al., 2007), since there is no significant change in

expression of BMP signaling-target genes such as *Pax6* that are typically involved in neural tube development (Liu and Niswander, 2005). This alternate pathway could explain the observed impairments in learning and memory that occur in PS1/CCL2KO mice despite up-regulation of *Nog*. Indeed, impairments in learning and memory are well associated with reduced c-fos$^+$ neurons, calbindin expression, and LTP (Kiyota et al., 2011; Molinari et al., 1996; Palop et al., 2003). This suggests that such changes in c-fos, calbindin and LTP in PS1/CCL2KO mice reflect reduced synaptic plasticity and memory consolidation. Moreover, decreased *Fgf2* expression supports the aforementioned, since boosting *Fgf2* expression results in improved synaptic plasticity in the hippocampus of AD mice (Kiyota et al., 2011), which is a reflective result for our current study.

Overall, we demonstrate that PS1 FAD mutation results in impairments in hippocampal neurogenesis associated with memory dysfunction in concert with CCL2-deficiency. These impairments are caused by the PS1 mutation and the CCL2KO influence hippocampal synaptic plasticity. Taken together, these findings support the idea that CCL2 has a critical role in not only chemotaxis in general, but also in specification of cell fate in hippocampal neurogenesis. In parallel, the PS1/CCL2KO mice have the potential to be developed as a mouse model for hippocampal neurogenesis for multiple animal systems.

Funding sources

This study was supported in part by NIH; Grant Nos.: AG043540, DA028555, NS036126, NS034239, MH064570, NS043985, MH062261 and AG043540, and DOD; Grant No.: 421-20-09A (to H.E.G.), the Carol Swarts Emerging Neuroscience Fund, start-up funds from the Department of Pharmacology and Experimental Neuroscience, and the Shoemaker Award for Neurodegenerative Research (to T.K).

Conflict of interest

The authors declare no competing financial interest.

Acknowledgments

The authors thank our laboratory members for experiments, discussions and comments, Dr. K. Duff for providing PS1 mice (M146L line 6.2).

Appendix A. Supplementary data

Supplementary data associated with this article can be found, in the online version, at http://dx.doi.org/10.1016/j.bbi.2015.06.014.

References

Ables, J.L., Breunig, J.J., Eisch, A.J., Rakic, P., 2011. Not(ch) just development: notch signalling in the adult brain. Nat. Rev. Neurosci. 12, 269–283.
Aimone, J.B., Wiles, J., Gage, F.H., 2006. Potential role for adult neurogenesis in the encoding of time in new memories. Nat. Neurosci. 9, 723–727.
Anderson, E.R., Gendelman, H.E., Xiong, H., 2004. Memantine protects hippocampal neuronal function in murine human immunodeficiency virus type 1 encephalitis. J. Neurosci. 24, 7194–7198.
Arendash, G.W., Schleif, W., Rezai-Zadeh, K., Jackson, E.K., Zacharia, L.C., Cracchiolo, J.R., Shippy, D., Tan, J., 2006. Caffeine protects Alzheimer's mice against cognitive impairment and reduces brain beta-amyloid production. Neuroscience 142, 941–952.
Butovsky, O., Koronyo-Hamaoui, M., Kunis, G., Ophir, E., Landa, G., Cohen, H., Schwartz, M., 2006. Glatiramer acetate fights against Alzheimer's disease by inducing dendritic-like microglia expressing insulin-like growth factor 1. Proc. Natl. Acad. Sci. U.S.A. 103, 11784–11789.
Chevallier, N.L., Soriano, S., Kang, D.E., Masliah, E., Hu, G., Koo, E.H., 2005. Perturbed neurogenesis in the adult hippocampus associated with presenilin-1 A246E mutation. Am. J. Pathol. 167, 151–159.
Choi, S.H., Veeraraghavalu, K., Lazarov, O., Marler, S., Ransohoff, R.M., Ramirez, J.M., Sisodia, S.S., 2008. Non-cell-autonomous effects of presenilin 1 variants on enrichment-mediated hippocampal progenitor cell proliferation and differentiation. Neuron 59, 568–580.
Couillard-Despres, S., Winner, B., Schaubeck, S., Aigner, R., Vroemen, M., Weidner, N., Bogdahn, U., Winkler, J., Kuhn, H.G., Aigner, L., 2005. Doublecortin expression levels in adult brain reflect neurogenesis. Eur. J. Neurosci. 21, 1–14.
De Strooper, B., Iwatsubo, T., Wolfe, M.S., 2012. Presenilins and gamma-secretase: structure, function, and role in Alzheimer disease. Cold Spring Harb. Perspect. Med. 2, a006304.
Deng, W., Aimone, J.B., Gage, F.H., 2010. New neurons and new memories: how does adult hippocampal neurogenesis affect learning and memory? Nat. Rev. Neurosci. 11, 339–350.
Duff, K., Eckman, C., Zehr, C., Yu, X., Prada, C.M., Perez-tur, J., Hutton, M., Buee, L., Harigaya, Y., Yager, D., Morgan, D., Gordon, M.N., Holcomb, L., Refolo, L., Zenk, B., Hardy, J., Younkin, S., 1996. Increased amyloid-beta42(43) in brains of mice expressing mutant presenilin 1. Nature 383, 710–713.
El Khoury, J., Toft, M., Hickman, S.E., Means, T.K., Terada, K., Geula, C., Luster, A.D., 2007. Ccr2 deficiency impairs microglial accumulation and accelerates progression of Alzheimer-like disease. Nat. Med. 13, 432–438.
El Khoury, J.B., Moore, K.J., Means, T.K., Leung, J., Terada, K., Toft, M., Freeman, M.W., Luster, A.D., 2003. CD36 mediates the innate host response to beta-amyloid. J. Exp. Med. 197, 1657–1666.
Elder, G.A., Gama Sosa, M.A., De Gasperi, R., Dickstein, D.L., Hof, P.R., 2010. Presenilin transgenic mice as models of Alzheimer's disease. Brain Struct. Funct. 214, 127–143.
Gao, J., Wang, W.Y., Mao, Y.W., Graff, J., Guan, J.S., Pan, L., Mak, G., Kim, D., Su, S.C., Tsai, L.H., 2010. A novel pathway regulates memory and plasticity via SIRT1 and miR-134. Nature 466, 1105–1109.
Gaulden, J., Reiter, J.F., 2008. Neur-ons and neur-offs: regulators of neural induction in vertebrate embryos and embryonic stem cells. Hum. Mol. Genet. 17, R60–R66.
Ishizuka, K., Kimura, T., Igata-yi, R., Katsuragi, S., Takamatsu, J., Miyakawa, T., 1997. Identification of monocyte chemoattractant protein-1 in senile plaques and reactive microglia of Alzheimer's disease. Psychiatry Clin. Neurosci. 51, 135–138.
Kempermann, G., Jessberger, S., Steiner, B., Kronenberg, G., 2004. Milestones of neuronal development in the adult hippocampus. Trends Neurosci. 27, 447–452.
Kiyota, T., Gendelman, H.E., Weir, R.A., Higgins, E.E., Zhang, G., Jain, M., 2013. CCL2 affects beta-amyloidosis and progressive neurocognitive dysfunction in a mouse model of Alzheimer's disease. Neurobiol. Aging 34, 1060–1068.
Kiyota, T., Ingraham, K.L., Jacobsen, M.T., Xiong, H., Ikezu, T., 2011. FGF2 gene transfer restores hippocampal functions in mouse models of Alzheimer's disease and has therapeutic implications for neurocognitive disorders. Proc. Natl. Acad. Sci. U.S.A. 108, E1339–E1348.
Kiyota, T., Yamamoto, M., Xiong, H., Lambert, M.P., Klein, W.L., Gendelman, H.E., Ransohoff, R.M., Ikezu, T., 2009. CCL2 accelerates microglia-mediated Abeta oligomer formation and progression of neurocognitive dysfunction. PLoS ONE 4, e6197.
Koo, E.H., Kopan, R., 2004. Potential role of presenilin-regulated signaling pathways in sporadic neurodegeneration. Nat. Med. 10 (Suppl.), S26–S33.
Lee, J.H., Yu, W.H., Kumar, A., Lee, S., Mohan, P.S., Peterhoff, C.M., Wolfe, D.M., Martinez-Vicente, M., Massey, A.C., Sovak, G., Uchiyama, Y., Westaway, D., Cuervo, A.M., Nixon, R.A., 2010. Lysosomal proteolysis and autophagy require presenilin 1 and are disrupted by Alzheimer-related PS1 mutations. Cell 141, 1146–1158.
Lee, S.W., Clemenson, G.D., Gage, F.H., 2012. New neurons in an aged brain. Behav. Brain Res. 227, 497–507.
Liu, A., Niswander, L.A., 2005. Bone morphogenetic protein signalling and vertebrate nervous system development. Nat. Rev. Neurosci. 6, 945–954.
Lledo, P.M., Alonso, M., Grubb, M.S., 2006. Adult neurogenesis and functional plasticity in neuronal circuits. Nat. Rev. Neurosci. 7, 179–193.
Louvi, A., Artavanis-Tsakonas, S., 2006. Notch signalling in vertebrate neural development. Nat. Rev. Neurosci. 7, 93–102.
Malenka, R.C., Bear, M.F., 2004. LTP and LTD: an embarrassment of riches. Neuron 44, 5–21.
McKhann, G.M., Knopman, D.S., Chertkow, H., Hyman, B.T., Jack Jr., C.R., Kawas, C.H., Klunk, W.E., Koroshetz, W.J., Manly, J.J., Mayeux, R., Mohs, R.C., Morris, J.C., Rossor, M.N., Scheltens, P., Carrillo, M.C., Thies, B., Weintraub, S., Phelps, C.H., 2011. The diagnosis of dementia due to Alzheimer's disease: recommendations from the National Institute on Aging-Alzheimer's Association workgroups on diagnostic guidelines for Alzheimer's disease. Alzheimer's Dement. 7, 263–269.
Molinari, S., Battini, R., Ferrari, S., Pozzi, L., Killcross, A.S., Robbins, T.W., Jouvenceau, A., Billard, J.M., Dutar, P., Lamour, Y., Baker, W.A., Cox, H., Emson, P.C., 1996. Deficits in memory and hippocampal long-term potentiation in mice with reduced calbindin D28K expression. Proc. Natl. Acad. Sci. U.S.A. 93, 8028–8033.
Naert, G., Rivest, S., 2011. CC chemokine receptor 2 deficiency aggravates cognitive impairments and amyloid pathology in a transgenic mouse model of Alzheimer's disease. J. Neurosci. 31, 6208–6220.
Nixon, R.A., 2013. The role of autophagy in neurodegenerative disease. Nat. Med. 19, 983–997.
Palop, J.J., Jones, B., Kekonius, L., Chin, J., Yu, G.Q., Raber, J., Masliah, E., Mucke, L., 2003. Neuronal depletion of calcium-dependent proteins in the dentate gyrus is

tightly linked to Alzheimer's disease-related cognitive deficits. Proc. Natl. Acad. Sci. U.S.A. 100, 9572–9577.
Shi, C., Pamer, E.G., 2011. Monocyte recruitment during infection and inflammation. Nat. Rev. Immunol. 11, 762–774.
Shimazu, K., Zhao, M., Sakata, K., Akbarian, S., Bates, B., Jaenisch, R., Lu, B., 2006. NT-3 facilitates hippocampal plasticity and learning and memory by regulating neurogenesis. Learn Mem. 13, 307–315.
Sun, M., Thomas, M.J., Herder, R., Bofenkamp, M.L., Selleck, S.B., O'Connor, M.B., 2007. Presynaptic contributions of chordin to hippocampal plasticity and spatial learning. J. Neurosci. 27, 7740–7750.
Sun, Y.X., Minthon, L., Wallmark, A., Warkentin, S., Blennow, K., Janciauskiene, S., 2003. Inflammatory markers in matched plasma and cerebrospinal fluid from patients with Alzheimer's disease. Dement. Geriatr. Cogn. Disord. 16, 136–144.
Veeraraghavalu, K., Sisodia, S.S., 2013. Mutant presenilin 1 expression in excitatory neurons impairs enrichment-mediated phenotypes of adult hippocampal progenitor cells. Proc. Natl. Acad. Sci. U.S.A. 110, 9148–9153.
Wen, P.H., Hof, P.R., Chen, X., Gluck, K., Austin, G., Younkin, S.G., Younkin, L.H., DeGasperi, R., Gama Sosa, M.A., Robakis, N.K., Haroutunian, V., Elder, G.A., 2004. The presenilin-1 familial Alzheimer disease mutant P117L impairs neurogenesis in the hippocampus of adult mice. Exp. Neurol. 188, 224–237.
Winner, B., Kohl, Z., Gage, F.H., 2011. Neurodegenerative disease and adult neurogenesis. Eur. J. Neurosci. 33, 1139–1151.
Yoon, K., Gaiano, N., 2005. Notch signaling in the mammalian central nervous system: insights from mouse mutants. Nat. Neurosci. 8, 709–715.
Zhang, C., McNeil, E., Dressler, L., Siman, R., 2007. Long-lasting impairment in hippocampal neurogenesis associated with amyloid deposition in a knock-in mouse model of familial Alzheimer's disease. Exp. Neurol. 204, 77–87.
Zhao, C., Deng, W., Gage, F.H., 2008. Mechanisms and functional implications of adult neurogenesis. Cell 132, 645–660.